JOURNAL OF GEOPHYSICAL RESEARCH, VOL. 111, B08407, doi:10.1029/2005JB004000, 2006

Channel flow and the development of parallel-dipping normal faults

Thorsten J. Nagel[1] and W. Roger Buck[2]

Received 16 August 2005; revised 13 April 2006; accepted 28 April 2006; published 24 August 2006.

[1] In a series of numerical experiments, arrays of parallel-dipping normal faults formed only if the model contained a thin viscous layer sandwiched between the brittle, faulted layer on top and a lower boundary that resisted vertical displacement. With this particular vertical stratification, parallel-dipping faults developed even if the viscous layer had a shear-stress-free lower boundary condition. This observation contradicts previous studies relating parallel-dipping normal faults to consistent horizontal shear stress in the brittle layer. We explain the formation of parallel-dipping normal faults in our experiments through the properties of flow in a thin viscous channel and how this flow accommodates and delocalizes faulting in the brittle layer on top. First, for closely spaced normal faults, an array of parallel-dipping faults minimizes the viscous work rate (dissipation) in the viscous layer as it minimizes the distance between sources and sinks in the flow pattern. Second, a thin layer of moderate viscosity leads to the required formation of closely spaced single faults. A highly viscous substratum tends to reflect faults at the base of the brittle layer and hence promotes the formation of a local graben at each necking site in the brittle layer. With lower viscosities, a thick layer or a floating lower boundary condition usually leads to the formation of widely spaced core complexes in the brittle layer. Our scheme can explain varying dip polarity along strike, which is observed in many rift systems and difficult to explain through consistent shear stress.

Citation: Nagel, T. J., and W. R. Buck (2006), Channel flow and the development of parallel-dipping normal faults, *J. Geophys. Res.*, *111*, B08407, doi:10.1029/2005JB004000.

1. Introduction

[2] Wide continental rifting is usually accommodated through arrays of roughly parallel-striking normal faults. Rather than showing a random sequence of the two possible conjugate fault orientations, such fault arrays develop regular dip patterns. Groups of adjacent faults often show the same dip direction forming so-called dip domains. Conversely, normal faults may arrange to arrays with alternating dip directions, thus defining a succession of horsts and grabens. We are interested in what mechanisms drive the formation of parallel-dipping normal faults as compared to a sequence of horsts and grabens. Well-developed dip domains of evenly spaced faults are very common in rift zones such as the Basin and Range Province in the western United States or the Suez Rift in northern Egypt (Figure 1) and they are observed over several orders of magnitude in scale. However, arrays of parallel-dipping normal faults have been rarely produced in numerical experiments and in sandbox experiments only if particular asymmetric boundary conditions were applied [*Mandl*, 1987; *McClay and Ellis*, 1987; *Brun et al.*, 1994]. Therefore experimental studies on this topic proposed that simple, symmetric stretching would promote a horst-and-graben-type fault pattern while the formation of parallel-dipping normal faults would require an asymmetry in the boundary conditions [*Mandl*, 1987; *Brun et al.*, 1994]. Several observations summarized in the next paragraph question the general validity of this conclusion. In our numerical experiments, parallel normal faults can develop with symmetric boundary conditions and even with a shear-stress-free lower boundary if the model has a particular vertical stratification. We use the results of numerical experiments and theoretical arguments to infer some fresh ideas about the origin of parallel-dipping normal faults.

2. Previous Models

[3] Dip patterns of normal fault arrays were analyzed in a number of analog experimental studies [e.g., *Mandl*, 1987; *Vendeville et al.*, 1987; *McClay and Ellis*, 1987; *Brun et al.*, 1994; *Brun*, 1999]. Most of these studies used sand as an analogue for the brittle crust. The consistent result was that a brittle sand layer on top of a viscous layer would extend through a set of horsts and grabens if symmetrically stretched. Hence a sequence of horsts and grabens was considered as the favorable geometry under nonspecial conditions.

[4] A consensus emerged that parallel-dipping normal faults are promoted by asymmetric boundary conditions

[1]Geologisches Institut der Universität Bonn, Bonn, Germany.
[2]Lamont-Doherty Earth Observatory of Columbia University, Palisades, New York, USA.

0148-0227/06/2005JB004000$09.00

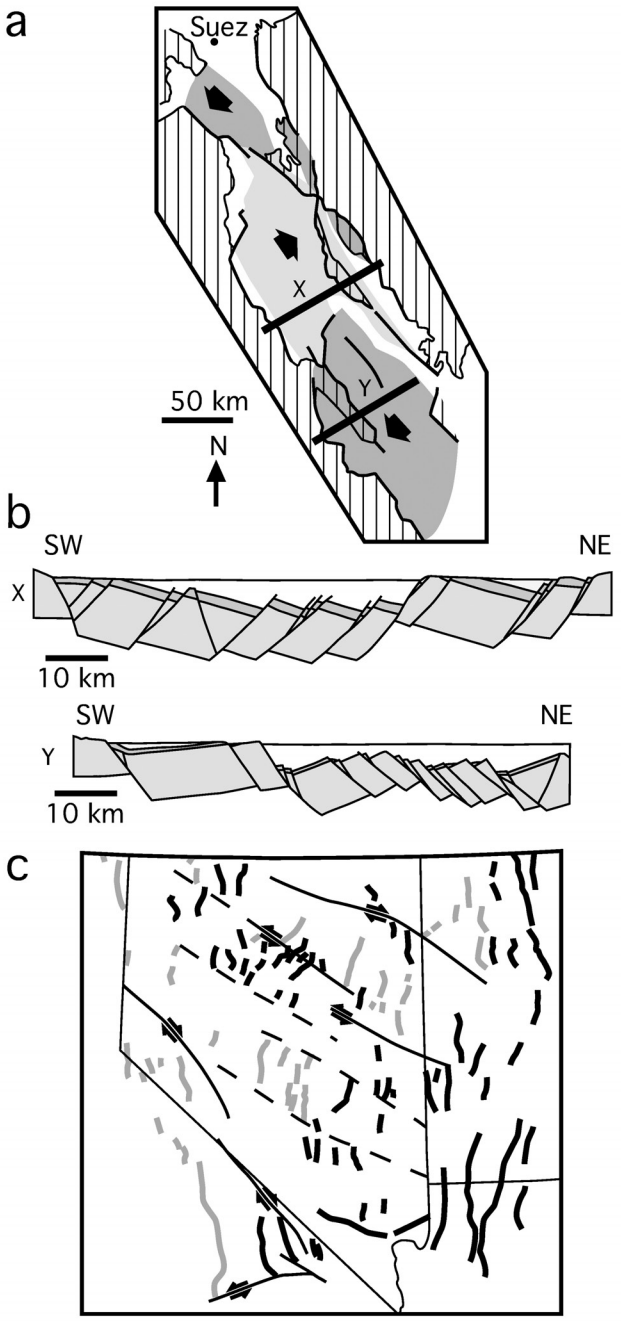

Figure 1. (a) Tectonic sketch of the Suez Rift in Egypt (simplified from *Coletta et al.* [1988], with permission from Elsevier). Hatched areas indicate exposure of prerift units (basement and sediments). Dark shading and light shading denote dip domains with southwestward and northeastward dipping fault arrays, respectively. (b) Cross sections X and Y indicated in Figure 1a (simplified from *Coletta et al.* [1988]). (c) Tectonic sketch of the Basin and Range Province, western United States [from *Stewart*, 1978]. Thin lines outline state borders. Thick shaded lines indicate ranges with dominant block tilting toward west (light shading) and toward east (dark shading), respectively.

leading to horizontal shear stress in the sand layer and an associated tilt of the stress trajectories. In experiments, this shear stress was imposed either through a topographic taper [*Mandl*, 1987; *McClay and Ellis*, 1987] or a consistent relative motion between the sand layer and its solid [*Mandl*, 1987] or viscous [*Brun et al.*, 1994] substratum. Figure 2 shows the result of a so-called two layer experiment with a viscous substratum [*Brun et al.*, 1994]: Sand and putty are placed in a box with rigid boundaries. As the right wall is suddenly removed, the sand collapses over the putty to the side. Faults in the sand predominantly dip in the direction toward the removed wall. The interpretation of the authors is that flow-related shear stress in the putty would produce a deflection of the stress trajectories in the lower part of the brittle layer and hence make one set of the conjugate normal faults kinematically favorable over the other. To produce the sense of shear favoring faults dipping toward the rift center requires a break in the brittle layer far from the rift center (where the wall was removed) and then development of faults closer to the center.

[5] So far, there are relatively few studies on parallel-dipping faults using numerical techniques. The above analysis was backed by numerical modeling of elastic bodies, from which *Melosh and Williams* [1989] inferred that the formation of a graben would release more elastic stresses than slip along two parallel-dipping faults. Some recent studies have produced arrays of parallel-dipping faults in numerical experiments where the brittle layer showed a pronounced lateral strength variation [*Behn et al.*, 2002; *Montesi and Zuber*, 2003a; *Nagel and Buck*, 2004]. In these experiments, fault dip was consistently directed toward the weakness. However, numerical models of faulting in a homogeneous layer usually produce arrays of horsts and grabens in zones of distributed extension [e.g., *Buck et al.*, 1999; *Walsh and Schultz-Ela*, 2003].

[6] There are a few observations that argue against flow-related horizontal shear stress or lateral strength variations being the exclusive factors for the formation of parallel-dipping normal faults. Some of the classical rift areas with parallel-dipping faults hardly have consistent lower crustal shear in the direction of fault dip nor do they show an obvious weak rift center. For example, the Basin and Range Province or the Suez rift (Figure 1) show varying dip polarities along strike with dip domains being separated by transform zones [*Stewart*, 1978]. For neither of these regions there is evidence that transfer zones correspond to reversals of the lower crustal flow direction with respect to the upper crust. Some experiments, especially ones using wet clay as a brittle material, produce parallel-dipping faults

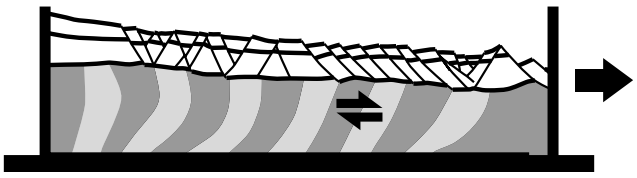

Figure 2. Two-layer sandbox experiment with asymmetric boundary conditions [from *Brun et al.*, 1994] leading to the formation of parallel-dipping faults. The lower boundary is rigid and attached to the left side of the model; the right side moves toward right. Length of the model is 15 cm.

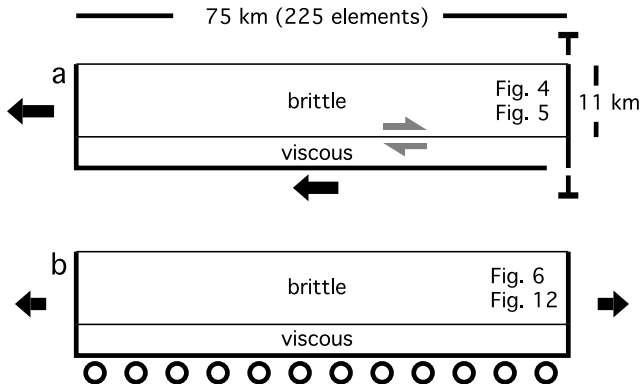

Figure 3. Schematic sketch of two different kinematic boundary conditions used in this study. (a) The setup that leads to a consistent motion between the bottom and the stretched brittle layer and associated right-lateral shear in the viscous lower layer. (b) The symmetric setup that excludes consistent shear through a free-slip lower boundary condition.

without any asymmetry in the boundary conditions or the material structure. Clay layers stretched on top of a homogeneously extending rubber sheet show the formation of dip domains and transfer zones that very much resemble natural examples [*Schlische et al.*, 2002; *Bellahsen et al.*, 2003]. It is not known why clay behaves so differently from sand and in some ways more like rocks at a crustal scale. In some tectonic settings the upper crust collapses over a viscous substratum into a weak rift center [*Brun and Beslier*, 1996; *Nagel and Buck*, 2004]. However, at lithospheric scales and for geologic rates of extension, asymmetric crustal collapse may not create substantial shear stress in the brittle crust. Crustal collapse into a localized necking area generates a topographic taper, as for example observed at continental margins. The pressure gradient associated with this topography drives flow in the viscous middle crust toward the depression in the rift center [*Block and Royden*, 1990; *Wernicke*, 1992]. In the upper part of the viscous middle crust, the shear stress applied to the base of the brittle layer due to this pressure-driven flow is opposite to that needed to produce faults dipping toward the rift center.

[7] In order to better understand what boundary and rheologic conditions produce parallel-dipping normal faults we carried out a series of numerical experiments to simulate fault development. These models build on previous work simulating normal faulting [e.g., *Poliakov and Buck*, 1998; *Lavier et al.*, 2000; *Buck et al.*, 1999; *Lavier and Buck*, 2002], but none of those studies looked at, or found, conditions leading to parallel sets of faults. The numerical method we use to simulate elastic, viscous and plastic deformation is an explicit finite difference scheme based on the FLAC method [*Cundall and Board*, 1988; *Cundall*, 1989; *Poliakov et al.*, 1993, 1994]. It is well described in the papers listed above. Two advantages of numerical models, compared to analog models, are that we can show stress and strain at all stages of deformation and almost any rheology for the brittle and viscous parts of the model can be specified. For example, we can define the rate of reduction in local brittle strength on a fault as a function of local strain needed to produce simulated faults (i.e., weak zones where strain is concentrated). Experiments shown in this study consist of two layers. The upper layer is always 11 km thick and has elastoplastic (brittle) properties following a Mohr-Coulomb failure criterion. The lower layer is a viscoelastic, Newtonian fluid with a vertically fixed lower boundary. Almost all experiments have the same horizontal size (75 km), grid resolution (3 elements per kilometer) and extension velocity (5×10^{-10} m s^{-1}). We varied thickness and viscosity of the lower layer and used two different kinematic boundary conditions (Figure 3). A few experiments have asymmetric boundary conditions with a lower boundary that moves with one of the walls leading to a consistent shear in the viscous layer (Figure 3a). However, most experiments have a free-slip lower boundary and are therefore perfectly symmetric. We will use these experiments to explore an alternative mechanism for the formation of parallel-dipping normal faults.

3. Numeric Experiments With Asymmetric Boundary Conditions

[8] The first task was to investigate the kinds of model geometries that produced parallel faults in the analog experiments. Figure 4 shows three experiments with a crustal-scale setup similar to the sandbox experiment shown in Figure 2 [*Brun et al.*, 1994]. The 11 km thick brittle layer lies on top of a 15 km thick Newtonian fluid. The stiff left and lower boundaries move with a velocity of 5×10^{-10} m s^{-1} to the left, the right wall is horizontally fixed. Along the lower boundary there is no vertical motion, along the walls at the side material can slip freely in the vertical direction. The singularity at the lower right corner is accommodated through localized stretching of three elements at the bottom of the viscous layer. The only varied parameter is the viscosity of the lower layer which is 5×10^{19}, 10^{20}, and 5×10^{20} Pa s, respectively. Neither experiment produces an array of parallel-dipping faults. Up to viscosities of 10^{20} Pa s the brittle layer extends by means of an asymmetric graben (Figures 4a and 4b). At the displayed stage after about 6 km of extension, only the prominent fault is active in both experiments and core complexes start to evolve. The orientation of the prominent fault is unsystematic and not determined by the asymmetry of the boundary conditions as the thick viscous layer does not transfer significant shear stress. With increasing viscosities, deformation starts to delocalize (Figure 4c); however, individual faults are reflected at the interface between the brittle and viscous layers leading to the formation of a graben-like structure.

[9] We reasoned that two conditions had to be met before parallel faults could form. First, parallel faults are a series of single faults that do not intersect other faults. This is in contrast to graben bounding pairs of faults. In earlier work on simulating normal faults, *Poliakov and Buck* [1998] proposed that single faults only occurred when the viscosity of the lower layer was lower than a given value (for many of their calculations with a 10 km thick brittle layer the cutoff for a constant viscosity lower layer was about 10^{19} Pa s). The second condition for parallel faults relates to the fact that extension has to be distributed on multiple faults and not localized on one fault. Viscous resistance seems the most likely way to get delocalization. Interaction with a

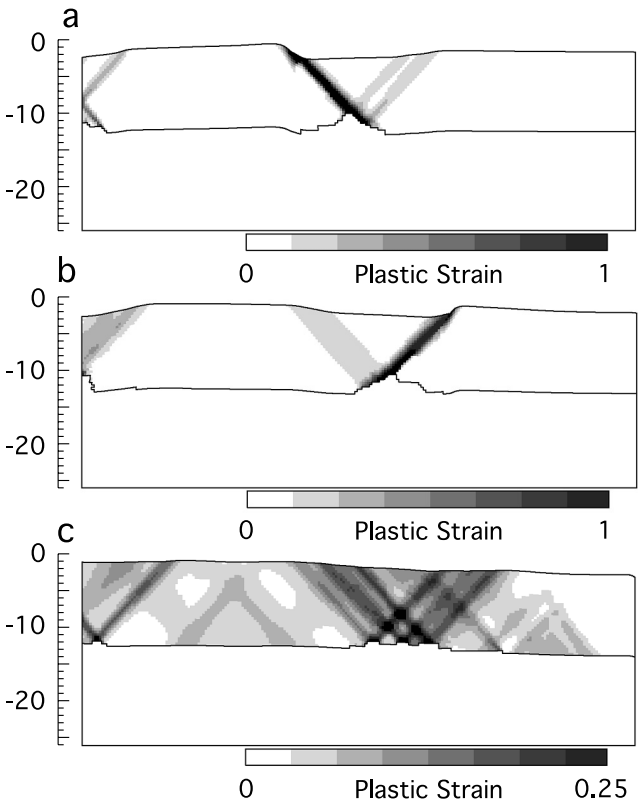

Figure 4. Two-layer numerical experiments with asymmetric boundary conditions similar to the setup in Figure 2, i.e., the right wall is fixed and the lower and left sides move toward the left. The extension velocity is 5×10^{-10} m s^{-1}. Each plot shows plastic strain after about 6 km extension. The models are 75 km wide and 26 km thick. The upper, brittle layer is 11 km thick, the lower, viscous layer 15 km, respectively. The viscosity of the lower layer is (a) 5×10^{19} Pa s, (b) 10^{20} Pa s, and (c) 5×10^{20} Pa s. The brittle material has a cohesion of 15 MPa and a friction angle of 30°. Brittle failure occurs according to a Mohr-Coulomb yield criterion. Where this criterion is met, the material deforms by means of a nonassociated plastic flow rule [*Poliakov and Buck*, 1998]. Localized plastic shear zones form as a result of arbitrary cohesion loss and a reduction of the friction angle with strain (between 1 and 100% strain cohesion is linearly reduced down to 5 MPa and the friction angle down to 25°). The mesh consists of 225×78 elements. Equations are solved using an explicit time marching, Lagrangian, finite difference scheme, a so-called FLAC scheme [*Cundall and Board*, 1988; *Cundall*, 1989; *Poliakov et al.*, 1993] that has been applied in many studies of crustal-scale extension [e.g., *Buck and Poliakov*, 1998; *Le Pourhiet et al.*, 2004; *Nagel and Buck*, 2004].

viscous substratum leads to dissection of the brittle layer into a series of fault-bounded blocks, a process often referred to as boudinage [*Ramberg*, 1955]. For a viscous layer of 10 or more km thickness, deformation usually remains localized at one site if viscosities are lower than 10^{20} Pa s. The problem is how to get viscous resistance sufficient to get effective delocalization (or boudinage) while still allowing single not graben-bounding faults between the less deformed blocks. As *Nagel and Buck* [2004] showed, having a thin, low-viscosity layer may allow development of a series of single faults that dip in the same direction; hence a thin viscous layer appears to delocalize deformation in the brittle layer more efficiently than a thick layer.

[10] Figure 5 shows an experiment with the same asymmetric boundary conditions as in Figure 4 but using an only 5 km thick lower layer with a viscosity of 10^{20} Pa s. Faulting initiates at the right side of the model and propagates toward left. After about 6 km of extension, an array of right-dipping faults has formed (Figure 5a). Strain rate (Figure 5b) and horizontal shear stress (Figure 5c) illustrate the flow pattern in the viscous layer. Considerable right-lateral shear is present only at the base of the channel, where shear flow and pressure-driven flow have the same sense of shear. At the top of the layer right-lateral shear stress is in the order of 1–2 MPa, which is about 1% of the total deviatoric stress. In the brittle layer, there is virtually no right-lateral background stress (white areas in Figure 5c indicate left-lateral component of horizontal shear stress). For layers thicker than a few kilometers even small topographic tapers lead to horizontal pressure gradients ($\partial p/\partial x$) and related pressure-driven flow (Poiseuille flow) that cancel the effect of the shear flow at the base of the brittle layer. As the brittle layer is stretched over the viscous substratum with a constant velocity, the shear velocity in the viscous channel is roughly defined by the boundary condition. Hence the strain rate ($\partial u/\partial y$) associated with shear flow (Couette flow) decreases with increasing channel thickness h, whereas the strain rate associated with opposite

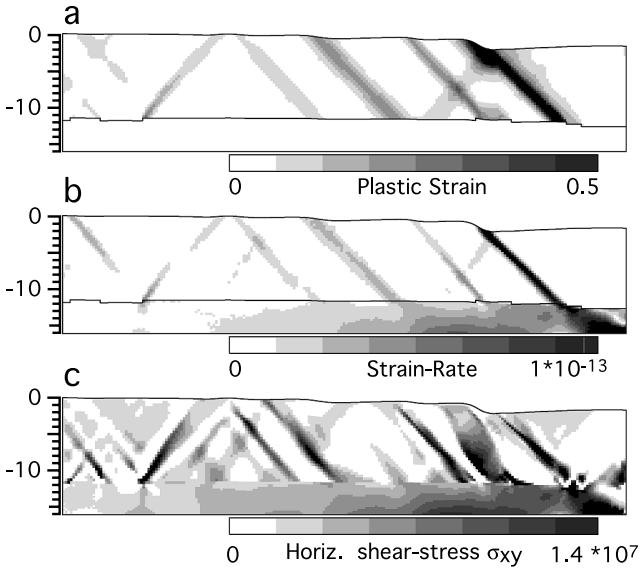

Figure 5. Two-layer numerical experiment with the same boundary conditions as in Figure 4. The viscosity of lower layer is 10^{20} Pa s. The only difference to experiment shown in Figure 4b is that the thickness of the lower layer is only 5 km. (a) Finite plastic (brittle) strain after about 6 km of extension. (b) Strain rate (plastic and viscous) at the same deformation stage. (c) Horizontal shear stress at the same deformation stage. Positive values denote right-lateral shear stress. Please note asymmetry of the scale.

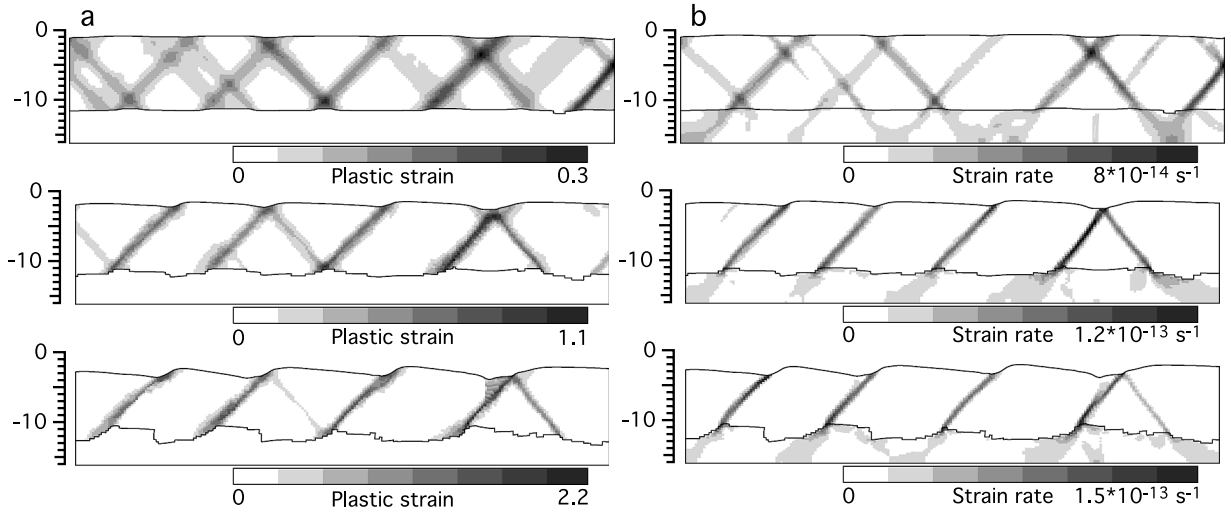

Figure 6. Two-layer numerical experiment with symmetric boundary conditions, i.e., a free-slip lower boundary condition. Model dimensions and material properties are the same as in the experiment shown in Figure 4. The extension velocity is again 5×10^{-10} m s^{-1}. (a) Plastic (brittle) strain after (top) 5, (middle) 10, and (bottom) 15 km of extension. Please note varying scales. (b) Strain rate (plastic and viscous) at the same deformation stages.

pressure-driven flow at the top of the channel ($y = 0$) increases,

$$\frac{\partial u}{\partial y} = \frac{1}{2\mu}\frac{\partial p}{\partial x}(2y - h) \tag{1}$$

with μ being the viscosity of the fluid [*Turcotte and Schubert*, 1982].

4. Numeric Experiments With Symmetric Boundary Conditions

[11] In our numerical experiments, parallel-dipping normal faults developed only if a relatively thin viscous channel was sandwiched between the brittle material on top and a lower boundary that resisted vertical displacement. However, if this condition was met, parallel faults formed even without any asymmetry in the boundary conditions. We typically used a lower boundary that was free of horizontal shear stress but vertically fixed. This boundary corresponds to a perfectly lubricated tabletop and is sometimes referred to as free-slip boundary condition. We chose this condition (rather than a homogeneously stretching lower boundary) in order to exclude consistent viscous shear as a result of strain localization in the upper layer. The experiment shown in Figure 6 has the same dimensions as the one in Figure 5. Again, an 11 km thick elastoplastic layer rests on top of a 5 km thick channel of a viscoelastic fluid with a viscosity of 10^{20} Pa s and the extension velocity is 5×10^{-10} m s^{-1}. After 5 km of extension (Figure 6a, top) several normal faults with small offsets have formed. Individual faults are reflected at the interface between the brittle and the viscous layer and the fault pattern can be viewed as a series of local grabens with the graben-defining faults intersecting at the bottom of the brittle layer. At the displayed early stage of deformation faults with both dip directions are active (Figure 6b, top). However, not all faults are active at the same time and activity may flip from one fault to another after some offset. For example, the left-dipping fault in the center of the model (Figure 6a, top) is hardly active at this particular moment (Figure 6b, top), but is restored soon afterward (Figures 6b, middle and 6b, bottom). After 10 km of extension the left-dipping faults of each local graben have accumulated more offset than the right-dipping ones and only left-dipping faults remain active (Figures 6a, middle and 6b, middle). Blocks between faults have started to tilt clockwise and the active faults rotate into shallower orientations. Once established, this fault pattern does not change with further extension (Figures 6a, bottom and 6b, bottom after 15 km of extension) and an array of parallel-dipping faults evolves. Hence, from a short early stage defined by a series of local grabens and varying individual fault activity the system switches into a stable mode, where only one fault of each graben remains active and these faults all dip in the same direction.

[12] In sections 5 and 6, we will analyze the reasons for closely spaced single faults arranging into a parallel-dipping array (section 5) and the conditions leading to closely spaced single faults (section 6). The second analysis includes the competition between failure along a single fault and paired faults forming a local graben (section 6.2) and a rough estimate of the wavelength of failure as a function layer thicknesses (section 6.3).

5. Analysis Part 1: Arranging Single Faults Into a Parallel-Dipping Array

[13] We consider a brittle layer that is extended on top of a thin viscous channel. The following analysis recognizes the two geometric elements of fault patterns mentioned before: the geometry of plastic necking (single-fault mode versus graben mode) and the wavelength of necking, i.e., the length of fault-bounded blocks. Figure 7 illustrates these geometric elements and possible combinations. In experi-

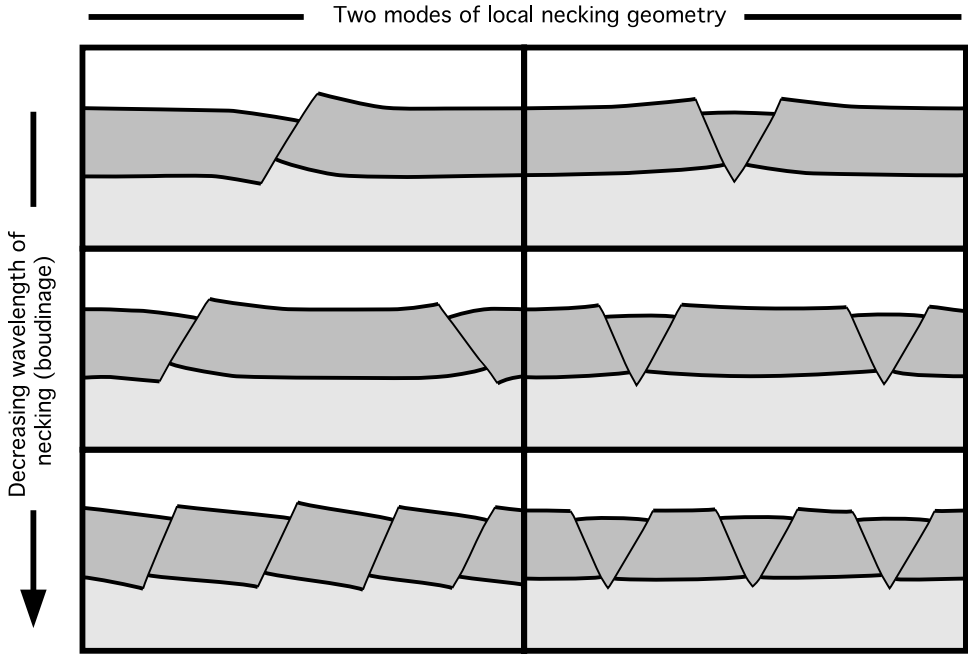

Figure 7. Conceptual sketch of fault patterns in a brittle layer extended on top of a viscous channel. We consider two different geometric elements: The wavelength of boudinage, i.e., the length of fault-bounded blocks (y axis) and the mode of failure (x axis, single-fault mode versus local graben mode). We observe the formation of parallel-dipping fault arrays only if failure occurs in a single-fault mode and individual faults are closely spaced, i.e., closer than the elastic wavelength of the brittle layer.

ments with a free-slip lower boundary condition, arrays of parallel-dipping faults formed only when necking occurred in a single-fault mode and the spacing between individual necks was particularly short, i.e., shorter than the elastic wavelength of the brittle layer. In this section we propose a mechanical explanation why closely spaced single faults might arrange to a parallel-dipping array rather than showing a random distribution of orientations.

[14] With closely spaced single faults, extension along a parallel-dipping array requires less viscous work rate (dissipation) in the underlying channel than a sequence of alternating faults. Figure 8 shows why this is so: Let us consider a brittle layer on top of a thin viscous channel, which fails by means of a series of evenly spaced single faults. Within the viscous channel material flows laterally from areas where blocks in the brittle layer drop down, i.e., hanging wall sections, toward areas where blocks pop up, i.e., footwall sections, and into necking sites, where blocks separate. Figure 8b images this flow pattern at the intermediate step of the shown experiment (Figures 6a, middle and 6b, middle) through the distribution of vertical deviatoric stress. Material is squeezed out of areas with negative vertical deviatoric stress into areas with positive vertical deviatoric stress. If faults all dip in the same direction the distance between narrowing and widening channel segments is particularly short, because each block has a hanging wall and a footwall section (Figure 8a, left). For opposite-dipping faults, dropping and raising sections have block length (Figure 8a, right). Hence, in a situation with opposite-dipping faults the channel length is on average twice as long as for parallel-dipping faults. We estimate the difference in work rate by considering a linear viscous channel of thickness h oriented parallel to the x axis (Figure 9). One side of the channel is deformed through a sinusoidal velocity field $v = v_0 \cos(kx)$ perpendicular to the channel axis. We assume that deformation of the boundary is accommodated by horizontal, pressure-driven flow in the channel (Poiseuille flow).

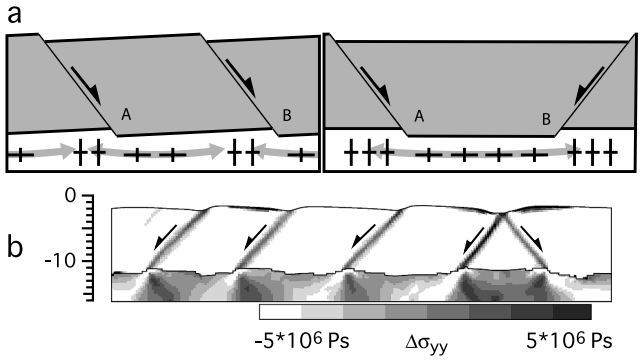

Figure 8. Schematic sketch of flow in a thin channel beneath a brittle layer failing by means of a series of evenly spaced normal faults. (a) Two adjacent faults that can have either (left) the same or (right) opposite dip directions. Material in the viscous channel flows laterally from areas beneath hanging walls into areas beneath footwalls. In the case of parallel-dipping faults, the average channel length is half as long as in the case of opposite-dipping faults. Arrows indicate flow directions, crosses stress trajectories. (b) Plot of vertical, deviatoric normal stress in the experiment shown in Figure 6 (step 2 after 10 km of extension). Negative values indicate vertical compression. Figure 8b shows that flow in the channel has indeed the geometry as proposed in Figure 8a (left).

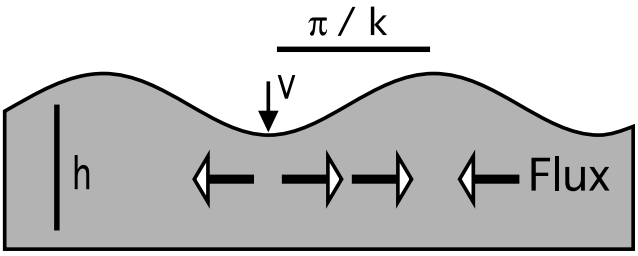

Figure 9. Sketch illustrating the model described by equations (2)–(5). One side of a thin, viscous channel with thickness h is deformed by a sinusoidal velocity field v. The distortion of the boundary is accommodated by pressure-driven flow (Poiseuille flow). Equation (5) shows the relation between the work rate associated with Poiseuille flow and the wavelength of the deformation field.

[15] Assuming mass conservation, the flux F through any cross section of the channel is

$$F = \bar{u}h = \frac{v_0}{k}\sin(kx) \tag{2}$$

with $\bar{u}$ being the average horizontal flow velocity [*Turcotte and Schubert*, 1982]. The pressure gradient associated with F is

$$\frac{dp}{dx} = -\frac{12\mu v_0}{kh^3}\sin(kx) \tag{3}$$

with μ being the viscosity of the fluid [*Turcotte and Schubert*, 1982]. It follows that

$$p = \frac{12\mu v_0}{k^2h^3}\cos(kx). \tag{4}$$

Hence the work rate $\partial W/\partial t = \int pvdx$ over a specific horizontal distance L is

$$\frac{\partial W}{\partial t} = \frac{12\mu v_0^2}{k^2h^3}\int_0^L \cos^2(kx)dx \tag{5}$$

and thus quadratically dependent on the length of the deformation cycle $2\pi/k$. In a channel of length L the work rate increases quadratically with decreasing wavelength of the sinusoidal deformation field. If this work rate is driven by extensional force applied from the side, the resulting difference in horizontal normal stress for a system like the one in Figure 6 is in the order of a few megapascals for each fault block. Note also the inverse cubic dependency between work rate and channel thickness h. Reducing the channel thickness, greatly increases the work rate. Section 6.3 treats the relation between the preferred wavelength of failure in the upper layer (which corresponds to the wavelength of the deformation field) and the channel thickness. We will show that decreasing the channel thickness results in a shorter wavelength of failure.

[16] We propose that parallel-dipping normal faults can form because of the associated short wavelength of widening and narrowing segments in the viscous layer. If this is true, the driving force for parallel-dipping normal faults would be related to vertical normal stress rather than horizontal shear stress. This scheme works only if blocks between normal faults behave rigidly, i.e., as long as the distance between two faults is smaller than the elastic wavelength of the brittle layer. Otherwise, the length of widening and narrowing channel segments would simply be determined by the elastic wavelength of the brittle layer and would not depend on fault orientations.

6. Analysis Part 2: Bringing Narrow Fault Blocks and Single Faults Together

6.1. Viscous Resistance and Strain Delocalization

[17] Fault patterns can be viewed in terms of delocalization of deformation. An offset increment along an existing fault can promote or impede further slip along the same fault [*Buck et al.*, 1999]. These effects are referred to as strain weakening or strain hardening, respectively. Strain weakening has the potential to localize deformation whereas strain hardening may cause delocalization, i.e., the formation of new faults. By definition, fault zones have to be weaker than undeformed material otherwise deformation would not much localize at all. In numerical models this is typically achieved through a strain dependency of parameters controlling the strength of the material, i.e., cohesion and friction angle. Another important strain-weakening effect is that slip along a normal fault thins the brittle layer which is usually the strongest part of the system. Conversely, fault offset is associated with bending of the brittle layer and distortion of the interface between the brittle layer and its surroundings, which usually requires work. Forces associated with this deformation resist further slip along the fault. Competition between strain-weakening and strain-hardening processes determines the fault pattern in the brittle layer [*Buck et al.*, 1999; *Lavier et al.*, 2000].

[18] A viscous substratum resists high deformation rates associated with localized faulting in the brittle layer and therefore generally has a delocalizing effect. In sections 6.2 and 6.3, we reflect on two different mechanism of viscous delocalization. First, large local stresses arise at the place where a fault hits the interface between the two layers. A confined area around the fault tip usually shows the highest deformation rates in the fluid (Figure 10). We believe that this local resistance contributes to the competition between single-fault mode and local graben mode, since the interface to a high viscous substratum tends to reflect faults in the upper layer [*Montesi and Zuber*, 2003b; *Huismans et al.*, 2005]. Second, viscous material has to accommodate for stretching and distortion of the interface at a larger scale. Particularly, it has to flow into the necking areas, where blocks in the brittle layer separate. This flow essentially determines the distance between sites of necking in the brittle layer, i.e., the wavelength of boudinage [e.g., *Ramberg*, 1955; *Biot*, 1961; *Smith*, 1975].

6.2. Single-Fault Mode or Local Graben Mode

[19] The geometry of local extensional failure, single-fault mode versus local graben mode, has been investigated in a few papers considering a brittle layer on top of an inviscid fluid [e.g., *Lavier et al.*, 2000]. With no viscous effects, forces resisting large offset along a single fault are

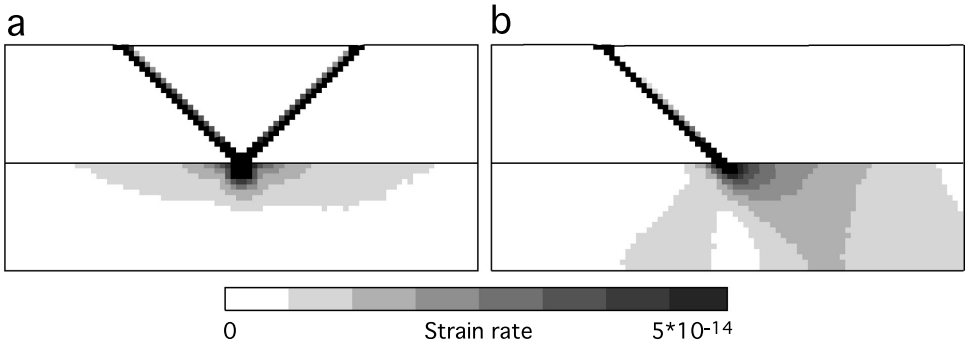

Figure 10. Two experiments with predefined faults. Brittle layer is 11 km thick; viscous layer is 10 km thick. The calculated experiment is 180 km wide (only the central part is shown); mesh size is 360 × 42 elements. Predefined faults are three elements wide and strengthless, i.e., cohesionless and frictionless. Plots show strain rate after 150 m of extension with a velocity of 2×10^{-10} m s^{-1}. (b) The experiment with a single predefined fault showing higher deformation rates in the viscous substratum than (a) the experiment with a predefined local graben.

related to bending of the brittle layer and the formation of topography. The result of these studies was that rapid fault weakening and thin layers would promote a single-fault mode, whereas strong layers and slow weakening would foster the formation of a local graben. The further effect of a viscous substratum has recently been investigated by *Huismans et al.* [2005]. In numerical experiments, Huismans et al. could induce transition from single-fault mode to local graben mode by increasing the viscosity of the lower layer. We, too, observe that raising the viscosity promotes the formation of local grabens. We propose that this behavior is related to viscous resistance around the tip of the fault, where it hits the interface between the brittle and the viscous layer [*Montesi and Zuber*, 2003b]. A local graben, two opposite-dipping faults that meet at the bottom of the brittle layer, allows the two brittle plates to separate with the least relative vertical offset at the lower boundary, i.e., the least distortion of the interface toward the viscous layer.

[20] Figure 10 shows two experiments designed to estimate the difference in viscous work rate of the two fault modes. Both experiments consist of an 11 km thick brittle layer on top of a 10 km thick linear viscous channel. The calculated model is 180 km wide (only the central part is shown in Figure 10). In order to estimate the viscous contribution to the pull force necessary to extend the system, we predefined strengthless, three elements wide cuts forming a local graben (Figure 10a) or a single fault (Figure 10b) in the center of the model. Figure 10 shows strain rates after 150 m extension with a velocity of 2×10^{-10} m s^{-1}. Obviously, the local graben mode minimizes the viscous work rate. Figure 11 displays pull force at the brittle layer, i.e., integrated horizontal deviatoric stress, against total amount of extension for the two fault modes and three different viscosities. As faults are strengthless, the pull force is dominantly related to work in the viscous layer (to some extend also to the buildup of topography and bending of the brittle layer). We propose that the early nonlinear behavior is related to the elastic stress buildup of the system – during the initial phase of the experiment, not all extension is accommodated at the predefined faults, especially not in experiments with high viscosities. For example at the stage displayed in Figure 10, the single fault accommodates only about 100 m of the bulk extension (150 m). However, after an initial phase the pull force increases linearly with offset for both fault modes and also appears to be linearly dependent on the viscosity of the lower layer.

[21] The difference in pull force between the two modes is as high as 9×10^{12} N for a substratum with a viscosity of 10^{20} Pa s and this relatively high extension rate. This corresponds to an average stress difference of 8 MPa. The response of the viscous substratum generally favors the graben mode, as the single-fault mode has to pay a viscous penalty. This penalty increases with viscosity of the substratum. Thus the interface between the brittle and the

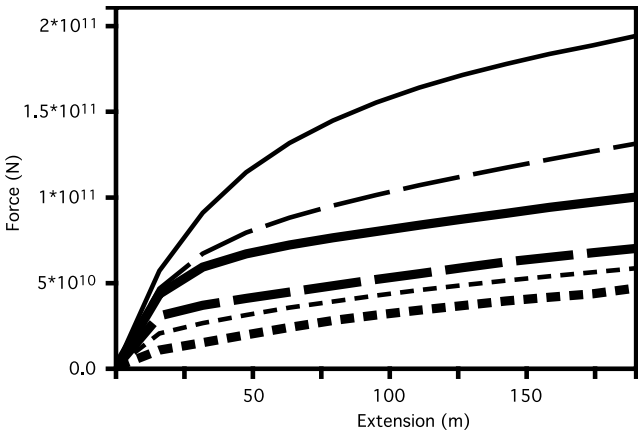

Figure 11. Pull force at the brittle layer versus bulk extension for six experiments with boundary conditions like the ones shown in Figure 10. Same line patterns indicate same viscosities of the substratum (undashed lines, 10^{20} Pa s; long dashed lines, 5×10^{19} Pa s; short dashed lines, 10^{19} Pa s). Thick lines indicate predefined local graben; thin lines indicate predefined single fault. After some extension, pull force rises linearly with offset and is linearly dependent on viscosity. For same viscosities, single faults require considerable more pull than local grabens.

viscous layer has a potential to reflect a fault. This also explains why graben-defining faults often appear to intersect close to the brittle ductile transition. As mentioned above, further properties such as the thickness and elastic strength of the brittle layer and the parameters controlling plastic strain weakening strongly influence the geometry of faulting. Rapid and ample strain weakening as well as thin layers promote the single fault mode [*Lavier et al.*, 2000]. The actual geometry of failure is determined by the competition between effects promoting one or the other mode. The setup for the experiments shown in Figures 4–6 was designed in a way that promotes the formation of single faults, particularly through the relatively small thickness of the brittle layer.

6.3. Boudinage on Top of a Thin Viscous Channel

[22] Continuum mechanics and instability analysis have been used to predict characteristic wavelengths of necking and buckling in stratified, viscous materials [*Biot*, 1961, 1965; *Smith*, 1975; *Fletcher and Hallet*, 1983]. Recently, *Montesi and Zuber* [2003b] have analyzed instabilities in a plastic layer on top of a viscous material in order to predict fault spacing. We cannot accurately predict the wavelength of faulting in our numerical experiments with analytical models. Many experiments show a complex evolution with varying numbers of active faults over time. However, for typical upper crustal thicknesses (10–15 km) and midcrustal viscosities (10^{19}–10^{20} Pa s) we usually yield necking wavelengths larger than the elastic wavelength of the brittle layer if the model has a floating lower boundary (Winkler Foundation) and/or rests on top of a thick viscous channel (Figures 12a and 12b). Such experiments have a tendency to develop widely spaced core complexes as viscous material can be easily pulled up from below. As the wavelength of folding or necking of a strong layer (viscous or elastic) in a viscous half-space depends on the strength ratio of the two materials it should be possible to obtain close fault spacing by reducing the strength ratio of the upper and lower layer. This could be achieved by increasing the viscosity of the lower layer. In numerical experiments similar to ours, *Bellahsen et al.* [2003] observed increasing delocalization, i.e., narrower fault spacing, as a result of increasing strain rates. This corresponds to increasing viscosities since higher strain rates enlarge flow stresses in the viscous material while leaving the strength of the brittle layer unaffected. However, as seen above higher viscosities promote the formation of local grabens in our experiments and with viscosities in excess of 10^{21} Pa s the resistance of the viscous material even starts to suppress the formation of localized shear zones at all [see *Huismans et al.*, 2005]. We find that thinning the viscous layer is an efficient way to delocalize deformation in the brittle layer, i.e., to reduce the wavelength of necking, without posing too much resistance at the fault tip (Figures 12a and 12b). The work rate associated with horizontal flow in a narrow channel has an inverse cubic dependency on the channel thickness (equation (5)). The viscous penalty resulting from a thin layer is buffered by the system through a smaller wavelength of necking. This relation can be shown analytically using the classic analysis of *Biot* [1961, 1965]. We compare folding (necking) of a viscous layer with a viscosity μ_1 and a thickness h_1 embedded in (1) a viscous half-space of viscosity μ_0 [*Biot*, 1961, 1965] and (2) between two narrow viscous layers of thickness h_0 and viscosity μ_0. The general differential equation for bending of a thin viscous plate is

$$\frac{\mu h^3}{3}\frac{\partial^5 w}{\partial^4 x \partial t} = q - \overline{P}\frac{\partial^2 w}{\partial x^2} \tag{6}$$

with w being displacement, q being vertical load per unit length, and P being a horizontal end load [*Turcotte and Schubert*, 1982]. We assume that displacement is given by [*Turcotte and Schubert*, 1982]

$$w = w_0 \cos\left(\frac{2\pi x}{\lambda}\right) e^{\frac{t}{t_a}} \tag{7}$$

The resistance (pressure) q associated with a displacement field w is

$$q = -4\mu_0\left(\frac{2\pi}{\lambda}\right)\frac{\partial w}{\partial t} \tag{8}$$

for viscous half-spaces on both sides of the layer [*Turcotte and Schubert*, 1982] and

$$q = -6\mu_0\left(\frac{\lambda^2}{\pi^2 h_0^3}\right)\frac{\partial w}{\partial t} \tag{9}$$

for thin layers of thickness h_0 on both sides [*Turcotte and Schubert*, 1982]. Note the very different dependency on λ for the two flow regimes. Substituting equations (7) and (8)–(7) and (9), respectively, into equation (6) yields [*Turcotte and Schubert*, 1982]

$$t_a = \frac{1}{\overline{P}}\left[\frac{2\lambda}{\pi}\mu_0 + \frac{4\pi^2}{3\lambda^2}\mu_1 h_1^3\right] \tag{10}$$

and

$$t_a = \frac{1}{\overline{P}}\left[\frac{4}{3}\pi^2\frac{\mu_1 h_1^3}{\lambda^2} + \frac{3}{2\pi^4}\frac{\lambda^4\mu_0}{h_0^3}\right] \tag{11}$$

respectively. The fastest growing wavelength λ can be obtained by setting the derivative of t_a with respect to λ equal to zero. The result is

$$\lambda = 2\pi h_1\left(\frac{1}{6}\frac{\mu_1}{\mu_0}\right)^{1/3} \tag{12}$$

for the half-space calculation [*Biot*, 1961; *Turcotte and Schubert*, 1982] and

$$\lambda = \pi\left(\frac{4\mu_1}{9\mu_0}\right)^{1/6}(h_1 h_0)^{1/2} \tag{13}$$

for the calculation with two enclosing viscous layers. Hence folding (necking) of a strong layer within thin less viscous channels is much more sensitive to variations in channel

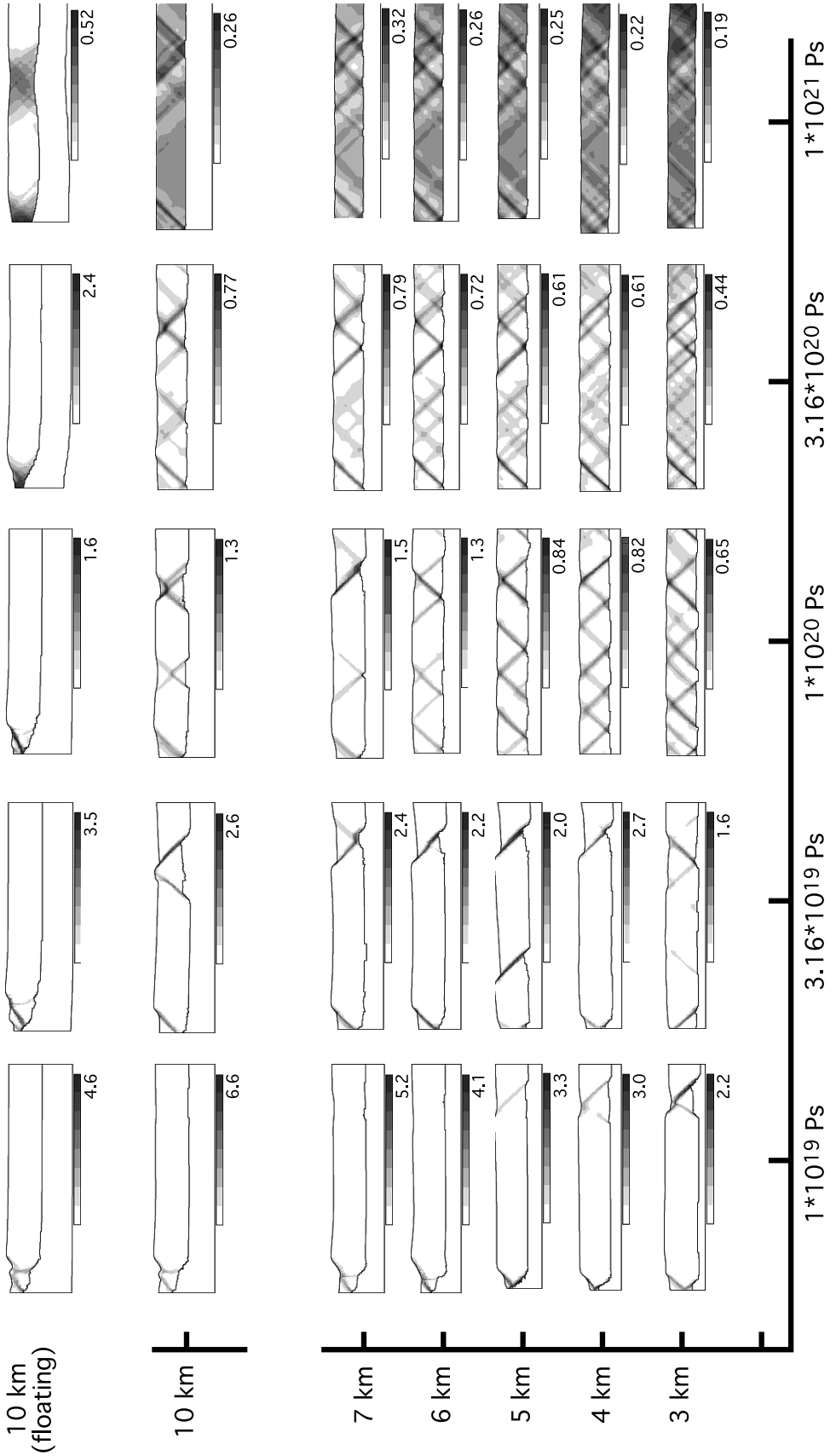
10 km (floating)
10 km
7 km
6 km
5 km
4 km
3 km
1*10^19 Ps
3.16*10^19 Ps
1*10^20 Ps
3.16*10^20 Ps
1*10^21 Ps
4.6
3.5
2.4
1.6
0.52
6.6
2.6
1.3
0.26
5.2
2.4
1.5
0.79
0.32
4.1
2.2
1.3
0.72
0.26
3.3
2.0
0.84
0.61
0.25
3.0
2.7
0.82
0.61
0.22
2.2
1.6
0.65
0.44
0.19

Figure 12a

thickness than to variations in viscosity. Of course, the above analysis is of limited quantitative value for our experiments as it considers only viscous rheologies. However, Figures 12a and 12b show that the prediction of equation (13) qualitatively applies also for our experiments with a plastic material on top of a viscous layer. Decreasing the thickness of the viscous layer proves at least as efficient to delocalize active faulting as does an increase of the viscosity. Thus a thin lower layer allows for narrowly spaced faults (bounding blocks or boudins) while still having a low enough viscosity in the layer as to promote the single-fault mode.

7. Discussion

7.1. Summary and Caveats

[23] In this paper we have shown that it is possible to get sets of parallel-dipping normal faults with no externally applied shear. In the numerical experiments done so far, arrays of parallel-dipping normal faults form only if the brittle, strain-weakening upper layer rests on top of a thin viscous channel with a strong lower boundary. With such a sandwich-like rheological stratification, parallel-dipping faults can develop even if the lower boundary is shear stress free. We explain this behavior by means of the vertical normal stress resistance in a thin viscous channel. The function of this channel is twofold. First, a thin channel accommodates displacement perpendicular to the channel wall with horizontal flow that is highly dependent on the horizontal wavelength of deformation (equation (5)). This wavelength is minimized by an array of parallel-dipping faults. Second, a thin channel explains closely spaced single faults in the brittle layer even if the viscosity is relatively low (equation (13)). High viscosities suppress the formation of parallel-dipping faults as they promote the reflection of individual faults at the interface between the brittle and viscous material. If a floating boundary condition or a channel thicker than a few kilometers was used, experiments did not develop the necessary close fault spacing for reasonable viscosities (Figures 4, 12a, and 12b). In about 100 experiments with free-slip lower boundaries we varied model parameters such as layer thickness, weakening parameters, viscosity, and extension velocity. Some experiments that produced relatively narrow fault spacing and a single-fault mode finally did not align all faults into a parallel orientation and we find it difficult to predict the specific behavior of an experiment beforehand. Faults usually do not form a parallel-dipping array from the start. As the experiments lack any sort of predefined weakness, the site of initial breaking is due to numerical effects. Often, the first faults form close to the edge of the model and dip inward, hence deformation starts with two opposite-dipping faults defining a wide graben. Strain weakening means that faults have a memory of past strain. Faults that have accumulated a certain offset may not be abandoned because of an unfavorable orientation. Also, fault delocalization, i.e., the development of fault arrays, is not just a result of viscous boudinage. Additional faults may form at places of strongest plate bending after some extension [*Lavier et al.*, 2000]. Therefore close fault spacing may also result from additional effects after some extension along wider spaced faults. However, Figures 12a and 12b testify that fault spacing in our experiments basically depends on the two considered parameters viscosity and thickness of the lower layer. Figure 12b (strain rate) consistently shows sets of single parallel-dipping faults in experiments with a thin channel ($\leq$6 km) and a moderate viscosity (1×10^{20} and 3.16×10^{20} Pa s). Instead, the finite strain plot (Figure 12a) indicates an increasing tendency to form local grabens toward higher viscosities (compare columns 1×10^{20} and 3.16×10^{20} Pa s in Figure 12a). At the displayed stage in Figure 12 (after 8 km of extension) all experiments in the critical parameter space (1×10^{20}/3.16×10^{20} Pa s/4–6 km layer thickness) have a locked orientation of active faults and the arrays of parallel-dipping faults intensify with further strain. However, it takes experiments with higher viscous substratum longer to arrest one set of parallel faults.

[24] Apart from the problems of initial breaking, our experiments face other numerical problems. The precise results of an experiment including the distance of fault spacing is to a certain degree dependent on grid size and size of time steps [*Poliakov et al.*, 1994]. Both parameters feed back into the process of strain weakening. Therefore we are unsure about the accuracy of our models concerning the quantitative relation between parameter space and failure modes. In the shown experiments the influence of grid size and time steps on fault spacing is small compared to the influence of the varied physical parameters (naturally, numerical parameters are the same for all experiments in Figure 12). Once established, parallel-dipping faults never change toward less organized fault patterns, whereas tight arrays of variously oriented faults usually arrange into a series of parallel-dipping faults after some extension.

[25] As the wavelength of boudinage depends on the strength ratio of the two layers it should also be possible two reduce fault spacing by changing the properties of the brittle layer such as cohesion, friction angle or pore pressure. In all our experiments, the brittle material follows Byerlee's law and is subjected only to a moderate reduction of the friction angle with plastic strain (from 30° down to 25°). Hence its strength is in the upper range of discussed values [*Scholz and Hanks*, 2004]. Lower initial friction

Figure 12a. Distribution of brittle strain in experiments with different viscous channel thickness (y axis) and viscosities (x axis). The upper brittle layer has a thickness of 11 km in all experiments and all experiments have the same boundary conditions as the experiment shown in Figure 6 (only the uppermost row shows experiments with a floating lower boundary, a so-called Winkler foundation, beneath a 10 km thick viscous layer). Stage shown is after approximately 8 km of extension. Fault spacing shows a dependency on both viscosity and viscous layer thickness. Sets of parallel-dipping faults develop in experiments with moderate viscosities and thin lower layers. See text for further discussion.

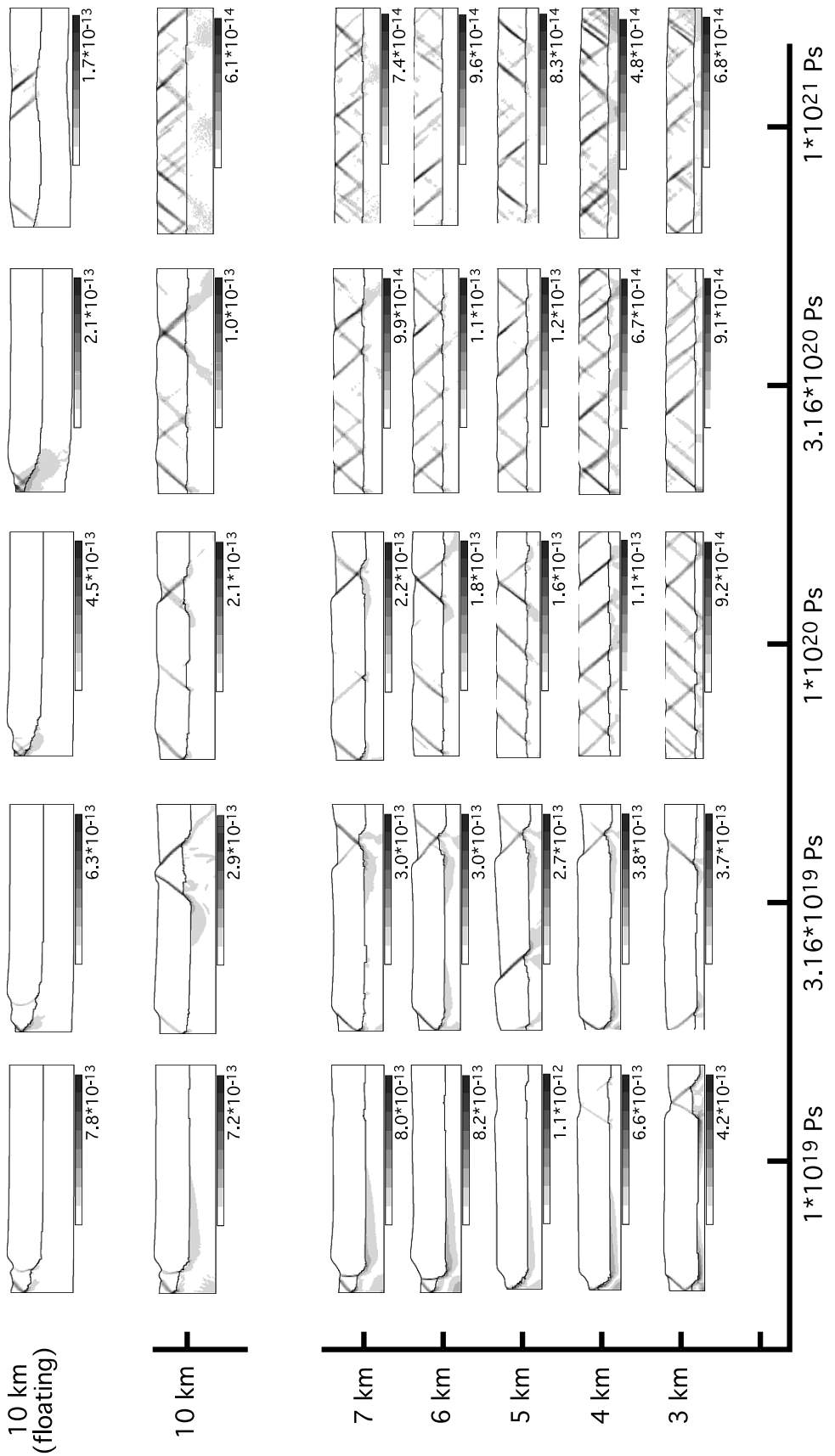

Figure 12b. Snap shots of strain rate (brittle and viscous) at the final stage of the experiments shown in Figure 12a. Strain rate is in unit strain per second. See text for further discussion.

angles and high pore pressures promote delocalization of deformation in our experiments and lead to closer fault spacing. Still, we have not obtained arrays of parallel-dipping faults with floating boundary conditions so far.

7.2. Thin Viscous Channels in Nature

[26] The shown experiments are designed in the spirit of physical experiments. Their very simple design is meant to test a mechanical hypothesis rather than to reproduce nature. The unrealistic free-slip lower boundary condition was chosen to ensure the absence of consistent shear in the viscous lower layer. A few experiments with homogeneously stretching lower boundaries yielded very similar results. Our theory might provide a new explanation for situations like the Suez rift or the Basin and Range Province where fault polarity of dip domains varies along strike and no rift center is apparent. This would imply that the brittle upper crust in these areas lies on top of moderately viscous middle crust that is not thicker than a few kilometers and has lower boundary with a certain stiffness. Hence the lower crust would have to be considerably stronger than the middle crust. Such a rheological stratification has been proposed on the basis of compositional variations and/or water depletion in the lower crust [e.g., *Kohlstedt et al.*, 1995]. A partly mafic and water depleted, i.e., granulite facies, lower crust is observed in the Ivrea zone in the southern Alps. There, the granulite facies metamorphism is associated with widespread Permian extension and magmatism similar to the Miocene situation in the Basin and Range Province. Thus the Ivrea lower crust was stronger than the middle crust during Permian extension [*Handy and Zingg*, 1991]. A resisting boundary between middle or lower crust may also arise from density differences with partly mafic lower crust being denser than granitic upper crust. In nature, arrays of parallel-dipping normal faults occur at very different scales. Obviously, the vast majority of them do not cut through the entire brittle crust. However, it appears that many arrays of parallel-dipping normal faults occur in stratified material and that faults often root in a thin weak layer such as salt or clay.

[27] **Acknowledgments.** We thank Laurent Montesi and an anonymous reviewer for their detailed and constructive reviews. The Department of Geodynamics in Bonn provided plenty of CPU time. This study was supported by grant Na411/1-1 of the German Science Foundation (DFG).

References

Behn, M. D., J. Lin, and M. T. Zuber (2002), A continuum mechanics model for normal faulting using a strain-rate softening rheology: Implications for rheological controls on continental and oceanic rifting, *Earth. Planet. Sci. Lett.*, *202*, 725–740.

Bellahsen, N., J.-M. Daniel, L. Bollinger, and E. Burov (2003), Influence of viscous layers on the growths of normal faults: Insights from experimental and numerical models, *J. Struct. Geol.*, *25*, 1471–1485.

Biot, M. A. (1961), Theory of folding of stratified viscolelastic media and its implications in tectonics and orogenesis, *Geol. Soc. Am. Bull.*, *72*, 1595–1620.

Biot, M. A. (1965), *Mechanics of Incremental Deformation*, 504 pp., John Wiley, Hoboken, N. J.

Block, L., and L. H. Royden (1990), Core complex geometry and regional scale flow in the lower crust, *Tectonics*, *9*, 557–567.

Brun, J. P. (1999), Narrow rifts versus wide rifts: Inferences for the mechanics of rifting from laboratory experiments, *Philos. Trans. R. Soc. London, Ser. A*, *357*(1753), 695–710.

Brun, J. P., and M. O. Beslier (1996), Mantle exhumation at passive margins, *Earth Planet. Sci. Lett.*, *142*, 162–173.

Brun, J.-P., D. Sokoutis, and J. van den Driessche (1994), Analogue modeling of detachment fault systems, *Geology*, *22*, 319–322.

Buck, W. R., and A. N. B. Poliakov (1998), Abyssal hills formed by stretching oceanic lithosphere, *Nature*, *392*, 272–275.

Buck, W. R., L. L. Lavier, and A. N. B. Poliakov (1999), How to make a rift wide, *Philos. Trans. R. Soc. London, Ser. A*, *357*(1753), 671–690.

Coletta, B., P. Le Quellec, J. Letouzey, and I. Moretti (1988), Longitudinal evolution of the Suez rift structure (Egypt), *Tectonophysics*, *153*, 221–233.

Cundall, P. A. (1989), Numerical experiments on localization in frictional materials, *Ing. Arch.*, *58*, 148–159.

Cundall, P. A., and M. Board (1988), A microcomputer program for modelling large-strain plasticity problems, in *Numerical Methods in Geomechanics*, edited by G. Swoboda, pp. 2101–2108, A. A. Balkema, Brookfield, Vt.

Fletcher, R. C., and B. Hallet (1983), Unstable extension of the lithosphere: A mechanical model for Basin and Range structure, *J. Geophys. Res.*, *88*, 7457–7466.

Handy, M. R., and A. Zingg (1991), The tectonic and rheological evolution of an attenuated cross section of the continental crust: Ivrea crustal section, southern Alps, northwestern Italy and southern Switzerland, *Geol. Soc. Am. Bull.*, *103*, 236–253.

Huismans, R. S., S. J. H. Buiters, and C. Beaumont (2005), Effect of plastic-viscous layering and strain softening on mode selection during lithospheric extension, *J. Geophys. Res.*, *110*, B02406, doi:10.1029/2004JB003114.

Kohlstedt, D. L., B. Evans, and S. J. Mackwell (1995), Strength of the lithosphere: Constraints imposed by laboratory experiments, *J. Geophys. Res.*, *100*, 17,587–17,602.

Lavier, L. L., and W. R. Buck (2002), Half graben versus large-offset low-angle normal fault: Importance of keeping cool during normal faulting, *J. Geophys. Res.*, *107*(B6), 2122, doi:10.1029/2001JB000513.

Lavier, L. L., R. W. Buck, and A. N. Poliakov (2000), Factors controlling normal fault offset in an ideal brittle layer, *J. Geophys. Res.*, *105*, 23,431–23,442.

Le Pourhiet, L., E. Burov, and I. Moretti (2004), Rifting through a stack of inhomogeneous thrusts (the dipping pie concept), *Tectonics*, *23*, TC4005, doi:10.1029/2003TC001584.

Mandl, G. (1987), Tectonic deformation by rotating parallel faults: The "bookshelf" mechanism, *Tectonophysics*, *141*, 277–316.

McClay, K. R., and P. G. Ellis (1987), Geometries of extensional fault systems developed in model experiments, *Geology*, *15*, 341–344.

Melosh, H. J., and C. A. Williams (1989), Mechanics of graben formation in crustal rocks: A finite element analysis, *J. Geophys Res.*, *94*, 13,961–13,973.

Montesi, L. G. J., and M. T. Zuber (2003a), Clues to the lithospheric structure of Mars from wrinkle ridge sets and localization instability, *J. Geophys. Res.*, *108*(E6), 5048, doi:10.1029/2002JE001974.

Montesi, L. G. J., and M. T. Zuber (2003b), Spacing of faults at the scale of the lithosphere and localization instability: 1. Theory, *J. Geophys. Res.*, *108*(B2), 2111, doi:10.1029/2002JB001924.

Nagel, T. J., and W. R. Buck (2004), Asymmetric alternative to asymmetric rifting models, *Geology*, *32*(11), 937–940.

Poliakov, A. N. B., and W. R. Buck (1998), Mechanics of stretching elastic-plastic-viscous layers: Application to slow-spreading mid-ocean ridges, in *Faulting and Magmatism at Mid-ocean Ridges*, *Geophys. Monogr. Ser.*, vol. 106, edited by W. R. Buck et al., pp. 305–323, AGU, Washington, D. C.

Poliakov, A. N. B., Y. Podladchikov, and C. Talbot (1993), Initiation of salt diapirs with frictional overburdens: Numerical experiments, *Tectonophysics*, *226*, 210–1999.

Poliakov, A. N. B., H. J. Herrman, Y. Y. Podladchikov, and S. Roux (1994), Fractal plastic shear bands, *Fractals*, *2*, 567–581.

Ramberg, H. (1955), Natural and experimental boudinage and pinch-and-swell structures, *J. Geol.*, *63*, 512–526.

Schlische, R. W., M. O. Withjack, and A. E. Clifton (2002), Effect of deformation rate on fault populations, *Geol. Soc. Am. Abstr. Programs*, *34*, 252.

Scholz, C. H., and T. C. Hanks (2004), The strength of the San Andreas Fault: A discussion, in *Rheology and Deformation of the Lithosphere at Continental Margins*, edited by G. D. Karner et al., pp. 261–383, Columbia Univ. Press, New York.

Smith, R. B. (1975), Unified theory of the onset of folding, boudinage, and mullion structure, *Geol. Soc. Am. Bull.*, *86*, 1601–1609.

Stewart, J. H. (1978), Basin-range structure in western North America: A review, in *Cenozoic Tectonics and Regional Geophysics of the Western Cordillera*, edited by R. B. Smith, and G. P. Easton, *Geol. Soc. Am. Mem.*, *152*, 1–32.

Turcotte, D. L., and G. Schubert (1982), *Geodynamics—Application of Continuum Physics to Geological Problems*, 450 pp., John Wiley, Hoboken, N. J.

Vendeville, B., P. R. Cobbold, P. Davy, J. P. Brun, and P. Choukroune (1987), Physical models of extensional tectonics at various scales, in *Continental Extensional Tectonics*, edited by M. P. Coward, J. F. Dewey, and P. L. Hancock, *Geol. Soc. Spec. Publ.*, *28*, 95–107.

Walsh, P., and D. D. Schultz-Ela (2003), Mechanics of graben evolution in Canyonlands National Park, Utah, *Geol. Soc. Am. Bull.*, *115*, 259–270.

Wernicke, B. (1992), Cenozoic extensional tectonics of the U.S. Cordillera, in *The Geology of North America*, vol. G-3, *The Cordilleran Orogen: Conterminous U.S.*, edited by B. C. Burchfiel, P. W. Lipman, and M. L. Zoback, pp. 553–581, Geol. Soc. of Am., Boulder, Colo.

W. R. Buck, Lamont-Doherty Earth Observatory of Columbia University, 61 Route 9W, P.O. Box 1000, Palisades, NY 10964-0190, USA.

T. J. Nagel, Geologisches Institut der Universität Bonn, Nussallee 9, D-53115 Bonn, Germany. (tnagel@uni-bonn.de)